

Neutron star equation of state and GW170817

Sajad A. Bhat and Debades Bandyopadhyay

Astroparticle Physics and Cosmology Division, Saha Institute of Nuclear Physics,
1/AF Bidhannagar, Kolkata-700064, India and Homi Bhabha National Institute,
Training School Complex, Anushaktinagar, Mumbai-400094

Abstract. Properties of neutron stars in GW170817 are investigated using different equations of state (EoSs) involving nucleons, Λ hyperons, quarks resulting in $2M_{\odot}$ neutron stars. This calculation is performed using the same EoS for merger components and for low spin prior case. It is found from the computations of tidal deformability parameters that soft to moderately stiff equations of state are allowed by the 50% and 90% credible regions obtained from the gravitational wave observation of binary neutron star merger GW170817, whereas the stiffest hadron-quark EoS which lies above the upper 90% limit, is ruled out. A correlation among the tidal deformabilities and masses is found to exist as already predicted. Furthermore moments of inertia and quadrupole moments of merger components of GW170817 are estimated.

Neutron stars, dense matter, equations of state, gravitational waves

Submitted to: *J. Phys. G: Nucl. Part. Phys.*

1. Introduction

The discovery of gravitational waves from the binary neutron star merger event GW170817 followed by the detection of its transient counterparts across the electromagnetic (EM) spectrum has heralded a new era in multimessenger astrophysics [1, 2]. The observed short Gamma Ray Burst (GRB) 1.7 s after the coalescence time provides clinching evidences for the association of short GRBs with neutron star mergers. This discovery of two colliding neutron stars and its aftermath led to plethora of information about short Gamma Ray Bursts, binary chirp mass, tidal deformability and dense matter in neutron star interior, speed of gravitational waves and heavy element synthesis due to r-process in ejected neutron-rich matter. The gravitational wave data led to the estimation of the binary chirp mass, $\mathcal{M}_{chirp} = (m_1 m_2)^{3/5} / (m_1 + m_2)^{1/5}$ in the 90% credible interval as $1.188^{+0.004}_{-0.002} M_\odot$ [1]. For low spin prior, the component masses of the binary lie in the range 1.17-1.6 M_\odot , whereas the total mass of the binary is $2.74^{+0.04}_{-0.01} M_\odot$. The binary mass ratio ($q = m_2/m_1$) is constrained in the range 0.7 - 1.0 for low spin prior. The optical/infrared transient, several hours after GW170817, was found to be consistent with emissions of a Kilonova which shines through radioactive decays of r-process nuclei synthesised in the neutron-rich ejected matter [3, 4].

The observation of GW170817 reveals many interesting aspects of dense matter in neutron stars and its equation of state (EoS). The fate of the compact remnant formed in the binary neutron star merger might be closely related to the amount of ejected material as estimated from EM signals [5]. A prompt collapse is ruled out by the quantity of blue kilonova ejecta observed in optical wavelengths. It is argued that the merger remnant was born as a hypermassive neutron star (HMNS) supported by differential rotation for a short duration of time. This picture of short lived HMNS might be consistent with the large quantity of red Kilonova ejecta, as observed in the infrared, originating from the accretion torus around the HMNS before its collapse to a black hole. The compact remnant spined down emitting gravitational waves and might have collapsed to a black hole close to the mass-shedding limit of uniformly rotating neutron stars [6]. This conclusion about the merger remnant leads to the upper bound on the maximum mass of non-rotating neutron stars and much tighter constraint on the EoS of dense matter [5, 6, 7, 8]. The lower bound on the maximum mass of neutron stars is obtained from pulsar observations.

It was long debated that the tidal effects in the late inspiralling phase of binary neutron stars could be large and detected by gravitational wave detectors [9, 10, 11]. The tidal deformation of a neutron star might provide crucial information about the dense matter EoS. The effective tidal deformability parameter is expected to be determined from gravitational wave signals. Indeed this was achieved in GW170817. The LIGO and VIRGO observations of GW170817 placed an upper limit on the dimensionless combined tidal deformability $\bar{\Lambda} \leq 800$ in the low spin case at 90% confidence level [1]. A lower limit on $\bar{\Lambda} \geq 400$ was estimated from the observational data

of the electromagnetic counterpart of GW170817 combined with numerical relativity simulations [7]. Recently another alternative approach involving radiative transfer simulations for the electromagnetic transient AT2017gfo predicts the lower bound on the tidal deformability to be $\bar{\Lambda} \geq 197$ [12].

Gravitational wave data of GW170817 were reanalysed by De et al. [13]. The initial analysis of the LIGO/VIRGO collaboration (LVC) differed from that of De et al. in the sense that the same EoS was not used for two neutron stars of GW170817 in the former case whereas in the latter case the tidal deformabilities (Λ_1 and Λ_2) and masses of both neutron stars were connected through the relation $\Lambda_1/\Lambda_2 \sim q^6$ implying that both neutron stars are described by the same EoS. Later the LVC analysed the data again using correlations in tidal deformabilities [14]. The correlation among tidal deformabilities led to a 20% reduction in 90% confidence upper bound of the effective tidal deformability [13, 14]. Tighter bounds on Λ_1/Λ_2 tuned to chirp mass are prescribed in an EoS-independent manner for gravitational waveform analysis [15].

The lower and upper bounds on the tidal deformability parameter put strong constraints on the dense matter EoS in neutron star interior. Radice et al. showed that too soft or too stiff EoSs were rejected because of those constraints [7]. Masses, radii and moments of inertia of neutron stars are the direct probes of dense matter EoS. The knowledge of tidal deformability from GW170817 was exploited to constrain the neutron star radius [13, 16, 17, 18, 19]. It was shown that the upper limit of the radius of a $1.4 M_\odot$ neutron star was ≤ 13.76 km [16]. In another investigation with one million different EoSs, the radius (R) of a $1.4 M_\odot$ neutron star is found to be $12.00 \leq R/\text{km} \leq 13.45$ [17]. Similar conclusion was drawn about the radius in Ref.[18]. Using the correlation among tidal deformabilities of merger components, radii of both neutron stars were constrained to be $8.7 < R/\text{km} < 14.1$ at the 90% credible interval [13]. The LVC also estimated the neutron star radii firstly adopting EoS-insensitive relations and secondly the same parameterized EoS for both neutron stars [19]. In the second case, the condition that the EoS was compatible with $1.97 M_\odot$ neutron stars was imposed. This led to higher radii of neutron stars in the second case than those of the first case [19]. So far we have noticed that gravitational wave data from GW170817 as well as its EM counterpart AT2017gfo led to the determination of upper bounds on the mass and radius of non-rotating neutron stars. Besides masses and radii of neutron stars, the measured tidal deformability could put constraints on other properties of merger components of GW170817 such as moment of inertia and quadrupole moment. This motivates us to explore EoS of dense matter and properties of merger components of GW170817 in this work.

This paper is organised in the following way. Equations of state used in this calculation are described in Sec II. We discuss results in Sec. III. We summarise our findings and conclude in Sec. IV.

2. Formalism

We discuss the computation of tidal deformability, moment of inertia and quadrupole moment in this section. These quantities are EoS dependent [20]. We adopt different relativistic mean field (RMF) models for the EoS of beta-equilibrated and charge neutral matter. The strong interaction among nucleons from the crust to the core is mediated by the exchange of scalar, vector and iso-vector mesons in these RMF models. The RMF parameterizations used in this calculations are TM1, TMA, SFHo, SFHx, DD2, DDME2 [21, 22]. An extended nuclear statistical model developed by Hempel and Schaffner (HS) is used to describe the matter in the sub-saturation density regime [23] along with the RMF nuclear interactions for the nonuniform and high density matter in all these cases. The SFHo and SFHx EoSs are fitted to some measurements of neutron star radii [24]. The density dependent (DD) couplings are used in the RMF models of nuclear interactions denoted by DDME2 and DD2 [22, 25]. The DD2 RMF model is extended to include Λ hyperons involving repulsive interaction mediated due to ϕ mesons, by Banik, Hempel and Bandyopadhyay (BHB) and is denoted as BHB $\Lambda\phi$ [26]. All the above mentioned EoSs are unified in the sense that the same RMF model used in the crust and core. Furthermore, these EoS are widely used for core collapse supernova and neutron star merger simulations. We consider also equations of state involving first-order phase transition from hadronic matter to quark matter. In one case, the hadronic phase including all hyperons and Δ resonance are described by the DD2 RMF model [27]. For the quark phase made of u, d and s quarks, a non-local extension of the Nambu-Jona-Lasinio model is employed [28]. Gibbs phase rules are imposed in the hadron-quark (HQ) mixed phase. We label this EoS as HQ1. The hadronic phase in other HQ EoS made of only nucleons is calculated using the NL3 RMF model whereas the quark phase is described by the effective bag model including quark interaction [29]. The HQ mixed phase in this case is based on the Maxwell construction. This EoS is denoted as HQ2.

A static and spherically symmetric star develops a quadrupole moment (Q_{ij}) in response to a static external quadrupolar tidal field ϵ_{ij} . The tidal deformability in the linear order is defined as $\lambda = -\frac{Q_{ij}}{\epsilon_{ij}}$. The $l = 2$ dimensionless tidal Love number k_2 related to λ is given by [10]

$$\lambda = \frac{2}{3}k_2R^5. \quad (1)$$

The spherically symmetric star under the linear $l = 2$, $m = 0$ perturbation due to the tidal field results in a static, even-parity perturbation of the metric which in the Regge-Wheeler gauge reduces to [10]

$$\begin{aligned} ds^2 = & -e^{2\Phi(r)} [1 + H(r)Y_{20}(\theta, \varphi)] dt^2 \\ & + e^{2\Lambda(r)} [1 - H(r)Y_{20}(\theta, \varphi)] dr^2 \\ & + r^2 [1 - K(r)Y_{20}(\theta, \varphi)] (d\theta^2 + \sin^2 \theta d\varphi^2), \end{aligned}$$

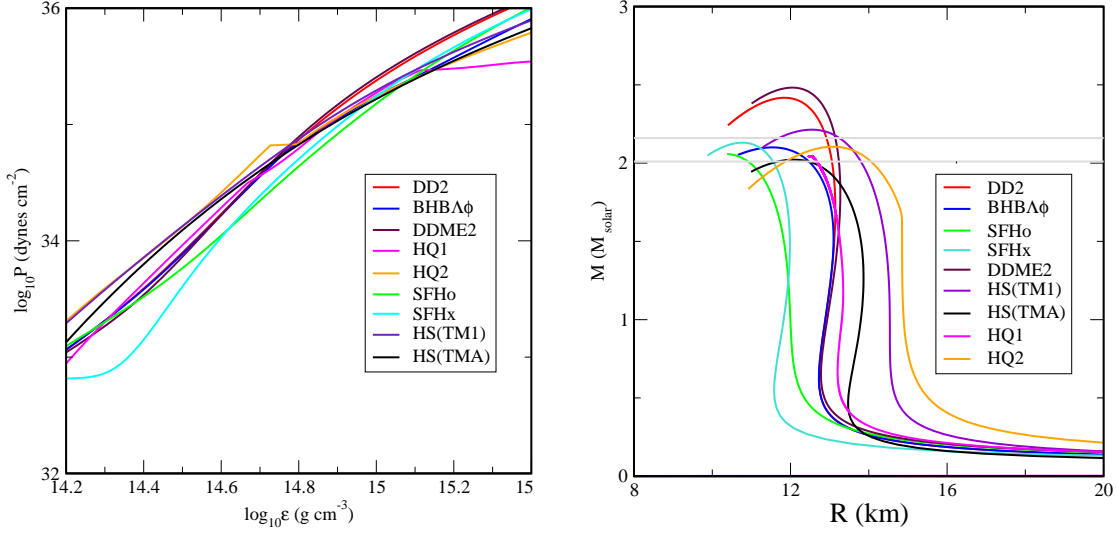


Figure 1. (Color online) Pressure versus energy density is shown for different compositions (left panel) and mass-radius relation is exhibited for those equations of state (right panel).

(2)

where, $K'(r) = H'(r) + 2H(r)\Phi'(r)$. Finally a second order differential equation for metric function H is obtained as

$$H'' + H' \left(\frac{2}{r} + \Phi' - \Lambda' \right) + H \left(-\frac{6e^{2\Lambda}}{r^2} - 2(\Phi')^2 + 2\Phi'' + \frac{3}{r}\Lambda' + \frac{7}{r}\Phi' - 2\Phi'\Lambda' + \frac{f}{r}(\Phi' + \Lambda') \right) = 0, \quad (3)$$

where, $f = d\epsilon/dp$. This equation is integrated outward from the center. Applying the asymptotic behaviour of $H(r)$, the $\ell = 2$ tidal love number is given by,

$$k_2 = \frac{8C^5}{5} (1 - 2C)^2 [2 + 2C(y - 1) - y] \times \left\{ 2C[6 - 3y + 3C(5y - 8)] + 4C^3[13 - 11y + C(3y - 2) + 2C^2(1 + y)] + 3(1 - 2C)^2[2 - y + 2C(y - 1)] \ln(1 - 2C) \right\}^{-1}, \quad (4)$$

$y = RH'(R)/H(R)$ and compactness of the star, $C = M/R$.

The dimensionless tidal deformability, dimensionless moment of inertia and dimensionless quadrupole moment are defined as $\Lambda_{1,2} = \frac{\lambda_{1,2}}{m_{1,2}^5}$, $\bar{I}_{1,2} = \frac{I_{1,2}}{m_{1,2}^3}$ and $\bar{Q}_{1,2} = \frac{Q_{1,2}}{(m_{1,2}^3 (J_{1,2}/m_{1,2}^2)^2)}$ respectively, where subscripts 1 and 2 correspond to masses of merger components, m_1 and m_2 respectively. Quadrupole moment $Q_{1,2}$ is compared with the Kerr solution quadrupole moment $J_{1,2}^2/m_{1,2}$ and the dimensionless $\bar{Q}_{1,2}$ are known as

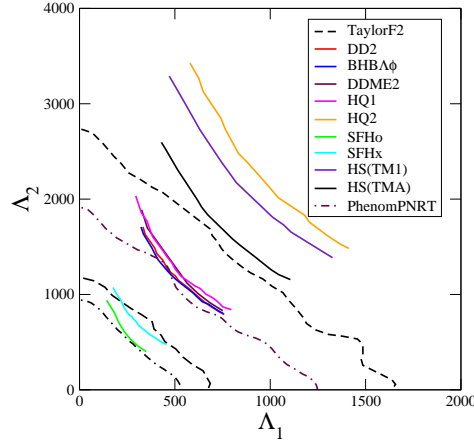


Figure 2. (Color online) Dimensionless tidal deformability parameters Λ_1 and Λ_2 are plotted here for different equations of state. Dashed and dash-dotted lines denote the 50% and 90 % probability contours as obtained from Ref.[1, 14].

Kerr factors corresponding to $m_{1,2}$. Moment of inertia and quadrupole moment are calculated by the spectral scheme within the numerical library LORENE [30, 31].

3. Results and Discussion

We adopt nuclear EoSs HS(TM1), HS(TMA), HS(SFHo), HS(SFHx), DDME2, HS(DD2), hyperon EoS BHBA ϕ and hadron-quark EoSs HQ1 and HQ2 for the calculation of neutron star properties as described in section II and shown in the left panel of Figure 1. The right panel of Figure 1 shows neutron star mass as a function of radius for the above mentioned EoSs. All those EoSs are compatible with $2 M_\odot$ neutron stars. We could learn valuable lessons about dense matter EoS from the fate of the massive remnant in GW170817. It is inferred that a hypermassive neutron star was born in the binary merger event and later it collapsed to a black hole. In this scenario, different groups estimated the upper bound on the maximum mass of non-rotating neutron stars (M_{max}^{TOV}) to be $2.16 M_\odot$ [5, 6, 8, 32]. On the other hand, the lower limit on the neutron star maximum mass $2.01 \pm 0.04 M_\odot$ was obtained from the observations of galactic neutron stars. Both bounds on the neutron star maximum mass i.e. $2.01 \pm 0.04 \leq M_{TOV}/M_\odot \leq 2.16 \pm 0.03$, put strong constraints on the EoS of dense matter. All EoSs except DD2, DDME2 and HS(TM1) satisfy these constraints on M_{max}^{TOV} as shown by two horizontal lines in the right panel of Fig. 1.

Tidal deformability Λ_2 is plotted with Λ_1 in Fig. 2 for all those EoSs considered here. Dimensionless tidal deformabilities of both merger components are calculated using the same EoS. It also shows the 50% and 90% credible intervals (dashed and dash-dotted lines) for the low spin case obtained using waveform models of TaylorF2 and PhenomPNRT [1, 14]. As the tidal deformability is directly proportional to R^5 , the

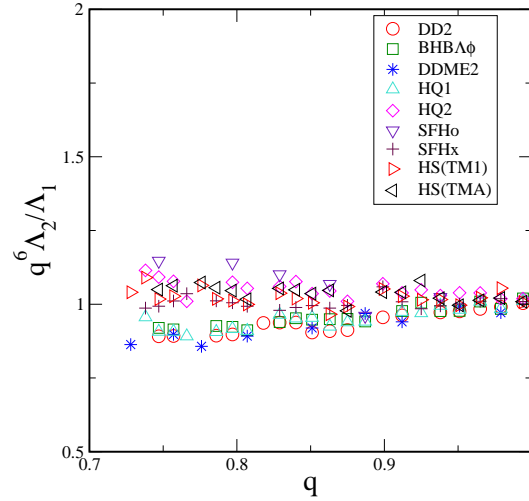


Figure 3. (Color online) The quantity $q^6 \Lambda_2 / \Lambda_1$ is shown as a function of mass ratio (q) for chirp mass $1.188 M_\odot$ and different equations of state.

compactness increases from top right corner to bottom left corner of Fig. 2. The SFHo EoS represents neutron stars with maximum compactness among all EoSs. The HQ2 EoS on the top right corner implies the least compact neutron stars and lies far outside the 90% credible interval. It is noted that HS(DD2) and BHBA ϕ EoSs which were allowed by TaylorF2 model, are now marginally compatible with the 90% contour of PhenomPNRT. The other EoSs which fall well inside 50% and 90% confidence intervals of PhenomPNRT are validated.

It has been noted that the tidal deformability parameter could probe the dense matter EoS. This can be further understood from Figs. 1 and 2. The upper limit on neutron star maximum mass is compatible with HQ2 and HS(TMA) along with several other EoSs as evident from Fig. 1. However, HQ2 and HS(TMA) EoSs are ruled out by the 90% confidence contour in Fig. 2. This demonstrates that the low density parts of HQ2 and HS(TMA) EoSs are not well constrained and lead to larger radii (> 14 km) for merger components. Besides this, the nuclear matter EoS in hadron-quark phase transition in HQ2 is described by the NL3 EoS which is very stiff. On the other hand, the neutron star maximum mass is estimated by the overall EoS which becomes softer due to the phase transition to quark matter.

A correlation among tidal deformabilities and mass ratio of neutron stars was reported by different groups [13, 14, 15]. When both neutron stars are described by the same EoS, it is found that tidal deformabilities follow the relation $\Lambda_1 / \Lambda_2 \sim q^6$ [13, 15]. Furthermore, analytical lower and upper bounds on Λ_1 / Λ_2 tuned to chirp mass were estimated studying large number of piecewise polytropic EoSs with and without strong first order hadron-quark phase transitions [15]. We investigate this correlation among tidal deformabilities and mass ratio for EoSs considered in Figs. 1 and 2. Figure 3 shows $q^6 \Lambda_2 / \Lambda_1$ as a function of mass ratio q . It is noted that this correlation holds

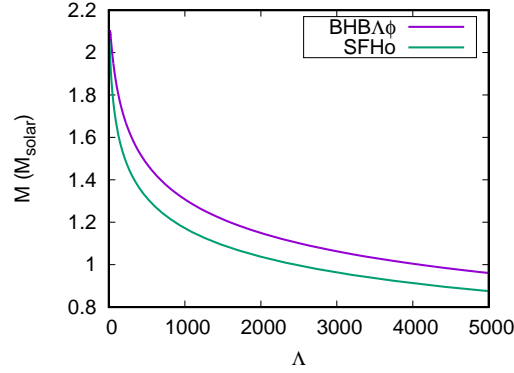


Figure 4. (Color online) Mass of neutron star is plotted as a function of tidal deformability for BHBA ϕ and SFHo equations of state.

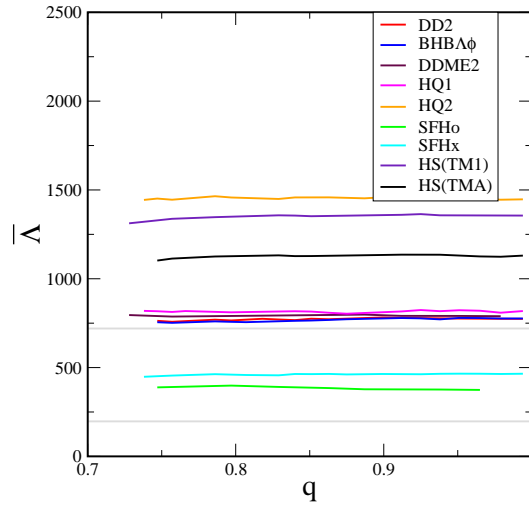


Figure 5. (Color online) Tidal parameter $\bar{\Lambda}$ is plotted against mass ratio q for a fixed chirp mass $\mathcal{M}_{chirp} = 1.188 M_{solar}$. Observational upper and lower limits (grey lines) are shown here.

good for values of mass ratio $q \geq 0.9$ for most EoSs adopted in this work. However, it is observed that the quantity $q^6 \Lambda_2 / \Lambda_1$ deviates from the value of unity for smaller values of q .

Neutron star mass is plotted as a function of individual tidal deformability for BHBA ϕ and SFHo EoSs in Fig. 4. The tidal deformability decreases as the neutron star becomes more massive. This also results in higher compactness. Consequently, more compact neutron stars will be less deformed. The tidal deformability for a $1.4 M_{\odot}$ neutron star is 697 and 334 in case of BHBA ϕ and SFHo EoSs, respectively.

LIGO and Virgo observations extracted the tidal contribution from the inspiral phase. The parameter ($\bar{\Lambda}$) that enters into the phase of the gravitational wave signal is

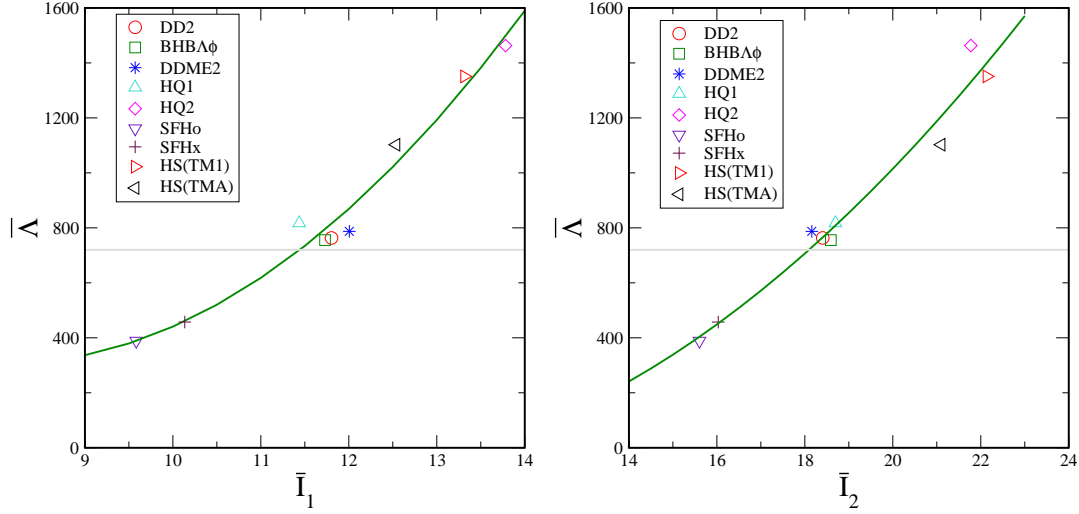


Figure 6. (Color online) Mass weighted average tidal deformability parameter $\bar{\Lambda}$ is shown as a function of dimensionless moment of inertia of the heavier component of the neutron star binary having mass $1.58 M_{\odot}$ (left panel) and for the lighter component of the neutron star binary having mass $1.18 M_{\odot}$ (right panel).

a mass-weighted linear combination of individual dimensionless tidal deformabilities as [33]

$$\bar{\Lambda} = \frac{16}{13} \frac{(m_1 + 12m_2)m_1^4\Lambda_1 + (m_2 + 12m_1)m_2^4\Lambda_2}{(m_1 + m_2)^5} \quad (5)$$

which is considered to be less than 720 at 90% confidence level [14] for low spin prior. Also an additional constraint placed on $\bar{\Lambda} \geq 197$ is based on EM observations of GW170817 [12]. So the allowed window for $\bar{\Lambda}$ is now $197 \leq \bar{\Lambda} \leq 720$.

Mass weighted average tidal deformability parameter $\bar{\Lambda}$ is plotted with the ratio (q) of masses of merger components for a fixed chirp mass $\mathcal{M}_{chirp} = 1.188 M_{\odot}$ in case of low spin scenario in Fig. 5. Here results are shown for all EoSs. Upper and lower boundaries on $\bar{\Lambda}$ that were obtained from the gravitational wave and EM observations, respectively, are also shown in Fig. 5. It is found that results corresponding to all EoSs satisfy the lower boundary. However, this can not be said about several EoSs with respect to the upper boundary. It is evident from Fig. 5 that HS(DD2) and BHBA ϕ EoSs are marginally outside the upper boundary whereas HS(TM1), HS(TMA), HQ1 and HQ2 EoSs are conclusively ruled out by the GW data. It is worth mentioning here that the estimates of both boundaries are strongly model dependent [7, 12, 14]. It is also noted from Fig. 5 that $\bar{\Lambda}$ is independent of q . This is also demonstrated analytically by Zhao and Lattimer [15].

We calculate gross properties such as moment of inertia and quadrupole moment of slowly rotating neutron stars with spin frequency 100 Hz in this calculation using

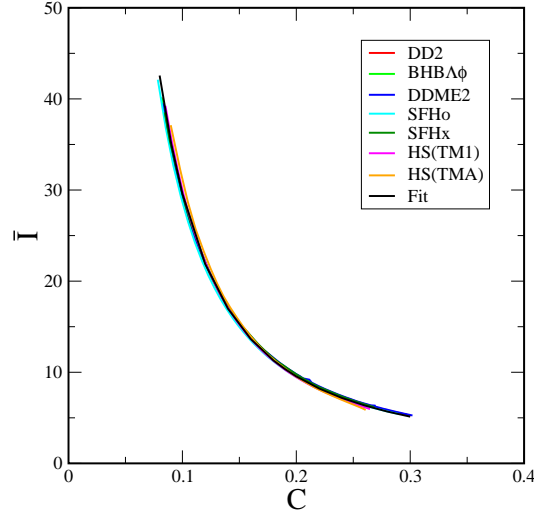


Figure 7. (Color online) Dimensionless moment of inertia is plotted with compactness of neutron star for different hadronic equations of state.

LORENE [30, 31]. Figure 6 shows the relations between the parameter $\bar{\Lambda}$ versus dimensionless moments of inertia of merger components \bar{I}_1 (left panel) and \bar{I}_2 (right panel), respectively. These results are obtained for masses of merger components ($m_1 = 1.58$, $m_2 = 1.18$) M_\odot as obtained from the chirp mass. The upper bound on $\bar{\Lambda}$ at 90% confidence level as obtained from gravitational wave data of GW170817 is also included on the plot. The intersections of the curves with the upper bound of $\bar{\Lambda}$ give upper limits on the values of moments of inertia of two merger components. The values of I_1 and I_2 so obtained are $\sim 2.0 \times 10^{45}$ g/cm² and $\sim 1.2 \times 10^{45}$ g/cm², respectively. These values of moments of inertia are consistent with the theoretically predicted values of Ref.[34].

As we know the moment of inertia and mass of each component, it is possible to estimate the radius of the corresponding component. This is done using the universal relation between dimensionless moment of inertia and compactness of neutron star [35]. This universal relation is shown in Fig. 7 for equations of state considered here except HQ EoSs in Fig. 7. The universal relation is fitted with the functional form as given by Eq. (20) of Ref. [35]. It is evident that the upper limit on the tidal deformability constrains radii of merger components to be ~ 13 km which are independent of component masses [18]. It is worth mentioning here that HQ EoSs violate the universality [20].

We do the similar investigation for quadrupole moments (Q_1 , Q_2) of merger components in GW170817. Figure 8 exhibits the behaviour of mass weighted average tidal deformability parameter with dimensionless quadrupole moments \bar{Q}_1 (left panel) and \bar{Q}_2 (right panel), respectively. The upper limit on $\bar{\Lambda}$ from gravitational wave observation of GW170817 is also shown in both figures. The values of upper bounds on

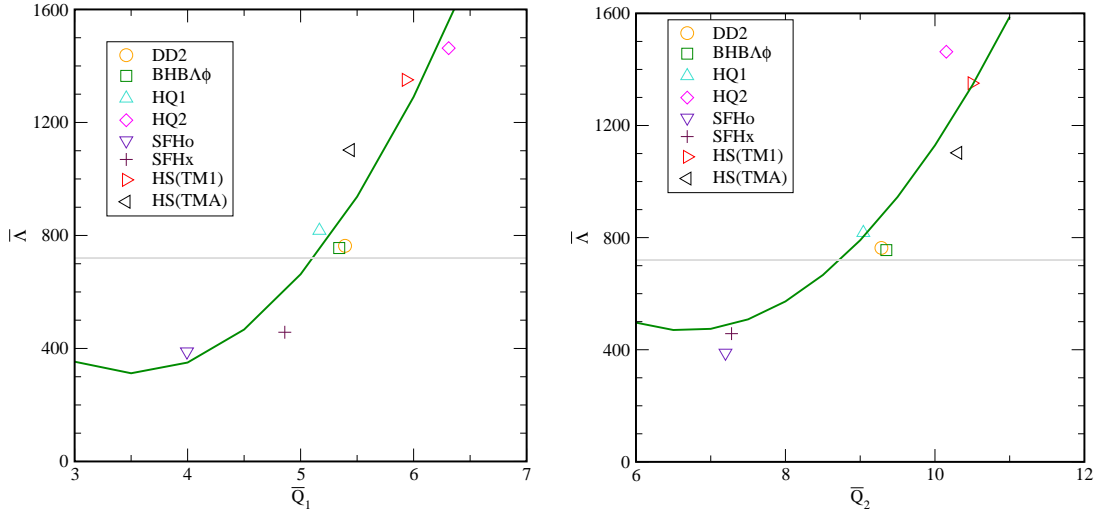


Figure 8. (Color online) Mass weighted average tidal deformability parameter ($\bar{\Lambda}$) is shown as a function of dimensionless quadrupole moment of the heavier component (left panel) and lighter component (right panel).

quadrupole moments are found to be in the range $0.29 - 0.30 \times 10^{43} \text{ g cm}^2$. Unlike the cases of moments of inertia in Fig. 6, the estimated value of upper bound on Q_1 is less than that of Q_2 because the latter merger component is less compact and it is easy to deform the star.

4. Conclusion

We investigate the constraints on EoS of neutron star matter and properties of merger components of GW170817. We exploit large number of EoSs involving nucleons, hyperons and quarks in this study. We compute mass-radius relation, tidal deformabilities, moment of inertia and quadrupole moment of the merger components using the same EoS. All those quantities are dependent on EoS. We find that 50 % and 90 % credible intervals on the mass weighted average tidal deformability parameter $\bar{\Lambda}$ obtained from gravitational wave data of GW170817 allow soft to moderately stiff EoSs. BHBA ϕ EoS might be allowed by 90% credible interval whereas too stiff EoS like HS(TM1), HS(TMA) and HQ2 are ruled out. It is also observed that tidal deformabilities and mass ratio of merger components satisfy $\Lambda_1/\Lambda_2 \sim q^6$ as predicted by other groups [13, 15]. Next we obtain upper bounds on moments of inertia and quadrupole moments of slowly rotating neutron stars exploiting the upper limit on the effective tidal deformability parameter $\bar{\Lambda}$ of GW170817. It has been possible to estimate radii of two merger components $\sim 13 \text{ km}$ as masses and moments of inertia of two merger components are known.

References

- [1] Abbott B P et al. 2017 Phys. Rev. Lett. **119** 161101
- [2] Abbott B P et al. 2017 Astrophys. J. Lett. **848** L13
- [3] Metzger B D Liv. Rev. Rel. 2017 **20** 3
- [4] Metzger B D et al. 2010 Mon. Not. R. Soc. **406** 2650
- [5] Margalit B and Metzger B D 2017 Astrophys. J. Lett. **850** L19
- [6] Rezzolla L, Moist E R and Weith L R 2018 Astrophys. J. Lett. **852** L25
- [7] Radice D, Perego A, Zappa F and Bernuzzi S 2018 Astrophys. J. Lett. **852** L29
- [8] Ruiz M, Shapiro S L and Tsokaros A 2018 Phys. Rev. D **97** 021501
- [9] Flanagan E E and Hinderer T 2008 Phys. Rev. D **77** 021502
- [10] Hinderer T 2008 Astrophys. J. **677** 1216
- [11] Hinderer T, Lackey B D, Lang R N and Read J S 2010 Phys. Rev. D **81** 123061
- [12] Coughlin M W et al. 2018 arXiv:1805.09371 [astro-ph]
- [13] De S et al. 2018 Phys. Rev. Lett. **121** 091102
- [14] Abbott B P et al. 2018 arXiv:1805.11579 [astro-ph]
- [15] Zhao T and Lattimer J M 2018 Phys. Rev. D **98** 063020
- [16] Fattoyev F J, Piekarewicz J and Horowitz C J 2018 Phys. Rev. Lett. **120** 172702
- [17] Moist E R, Weith L R, Rezzolla L and Schaffner-Bielich J 2018 Phys. Rev. Lett. **120** 261103
- [18] Raithel C, Özel F and Psaltis D 2018 Astro. Phys. J. **857** L23
- [19] Abbott B P et al. 2018 Phys. Rev. Lett. **121** 161101
- [20] Bandyopadhyay D, Bhat S A, Char P and Chatterjee D 2018 Eur. Phys. J. A **54** 26
- [21] Oertel M, Hempel M, Klähn T and Typel S 2017 Rev. Mod. Phys. **89** 015007
- [22] Lallazissis G A, Niksić T, Vretenar D and Ring P 2005 Phys. Rev. C **71** 024312
- [23] Hempel M and Schaffner-Bielich J 2010 Nucl. Phys. A **837** 210
- [24] Steiner A W, Hempel M and Fischer T 2013 Astrophys. J. **774** 17
- [25] Typel S et al. 2010 Phys. Rev. C **81** 015803
- [26] Banik S, Hempel M and Bandyopadhyay D 2014 ApJS **214** 22
- [27] Mellinger Jr R D, Weber F, Spinella W, Contrera G A and Orsaria M G 2017 Universe **3** 1
- [28] Orsaria M, Rodrigues H, Weber F and Contrera G A 2013 Phys. Rev. D **87** 023001
- [29] Mishustin I N, Mallick R, Nandi R and Satarov L 2015 Phys. Rev. C **91** 055806
- [30] Gourgoulhon E, Grandclément P, Marck J -A, Novak J and Taniguchi K 2016 LORENE spectral methods differential equation solver ascl:1608.018
- [31] <http://www.lorene.obspm.fr/>
- [32] Banik S and Bandyopadhyay D 2017 arXiv:1712.09760 [astro-ph]
- [33] Fatava M 2014 Phys. Rev. Lett. **112** 101101
- [34] Bhattacharyya S, Bombaci I, Bandyopadhyay D, Thampan A V and Logoteyta D 2017 New Astronomy, **54** 61
- [35] Breu C and Rezzolla L 2016 Mon. Not. R. Astron. Soc. **459** 646